Int. J. Heat Mass Transfer. Vol. 34, No. 10, pp. 2509–2519, 1991
Printed in Great Britain

0017–9310/91 $3.00 + 0.00
Pergamon Press plc

A comparison of models and experimental data for pressure drop and heat transfer in irrigated packed beds

M. S. BOHN
Solar Energy Research Institute, 1617 Cole Blvd., Golden, CO 80401, U.S.A.

and

L. W. SWANSON
Department of Engineering, University of Denver, Denver, CO 80208, U.S.A.

(*Received* 16 *July* 1990 *and in final form* 13 *November* 1990)

Abstract—This paper presents a comparison of experimental data with models of heat exchange and pressure drop in irrigated packed beds with special emphasis on determining the validity of the models, the importance of radiation heat transfer, and the effectiveness of such heat exchangers. Heat transfer and pressure drop are measured in a 150 mm (i.d.) column with a 610 mm bed of metal Pall rings. Molten nitrate salt and preheated air are the working fluids. Salt inlet temperatures ranging from 335 to 520°C and air inlet temperatures ranging from 215 to 380°C are tested. A comparison between the experimental data and a modified version of the heat transfer model of Bohn (*Proc. 2nd ASME–JSME Thermal Engng Conf.*, Honolulu, Hawaii (1987)) is made on the basis of heat transfer from the salt. For the range of air and salt rates tested, 0.3–1.4 kg m^{-2} s^{-1} air flow and 6–18 kg m^{-2} s^{-1} salt flow, the data agree with the model within 25% standard deviation. The role of radiation heat transfer is found to be relatively minor and the heat exchanger is found to behave essentially as a simple counterflow exchanger with a heat exchange effectiveness of unity. Two models for the column pressure drop are compared with the data over a pressure drop ranging from 160 to 1045 Pa m^{-1}. The standard deviation for the model of Stichlmair *et al.* (*Gas Separation Purification* **3**, 19–28 (1989)) is 9.4%; that for the model of Bemer and Kalis (*Trans. Instn Chem. Engrs* **56**, 200–204 (1978)) is 16.4%.

1. INTRODUCTION

IN MANY commercial processes it is necessary to bring liquid and gas streams into contact to allow the transfer of heat or mass between the two streams. Transferring mass between the two streams may be an end unto itself or it may be needed to carry out a chemical reaction at the gas/liquid interface. In many of these cases heat transfer occurs in parallel with mass transfer, and in several important applications, the transfer of heat may be the desired end result. In all cases momentum transport between the two streams is inevitable and results in pressure drop on the gas side. This pressure drop contributes to operating costs and thus is to be minimized. Examples of important industrial applications that utilize direct-contact mass transfer include:

- flue gas scrubbing;
- gas separation/scrubbing (e.g. CO_2, H_2S);
- chemical purification;
- separation of organic liquids;
- steam desorption/desuperheating;
- condensation;
- cooling towers;
- fractionation;
- desalination;
- removal of pollutants from buildings;
- food purification;
- contacting metal slags with gas streams in iron blast furnaces;
- manufacture of high-purity products (e.g. H_2SO_4, HNO_3);
- fermentation;
- hydrogenation;
- gasification and desulfurization of coal;
- cracking of coal extracts;
- chlorination of hydrocarbons.

Many industrial processes that involve heat transfer either currently use or effectively could use this technology. These can be categorized as applications in which energy is recovered, collected, or managed more effectively via the application of the heat exchanger:

- flue gas heat recovery;
- solar central receivers for high-temperature gas applications;
- hot gas quenching;
- water/oil quenching;
- electronic component cooling;
- gas preheating upstream of a chemical reactor vessel.

NOMENCLATURE

A_c	column cross-sectional area [m^2]
C_s	salt specific heat [J kg^{-1} K^{-1}]
C_{pa}	air specific heat [J kg^{-1} K^{-1}]
G	gas mass flow per unit cross-sectional area of empty column [kg m^{-2} s^{-1}]
f_0	single-particle friction factor
H	column height [m]
k	salt thermal conductivity [W m^{-1} K^{-1}]
L	salt mass flow per unit cross-sectional area of empty column [kg m^{-2} s^{-1}]
$\dot{m}_s$	salt mass flow rate [kg s^{-1}]
Q_{loss}	heat transfer from salt other than that to the air [W]
Q_{outlet}	heat transfer from salt to air below packed bed [W]
Q_s	heat transfer, salt to air [W]
Q_{sm}	measured heat transfer, salt to air, in packed bed [W]
Re_g	single-particle Reynolds number for the gas phase
T_{ai}	air inlet temperature [°C]
T_{ao}	air outlet temperature [°C]
T_{si}	salt inlet temperature [°C]
T_{so}	salt outlet temperature [°C]
Ua	volumetric heat transfer coefficient [W m^{-3} K^{-1}].

Greek symbols

μ	salt dynamic viscosity [kg m^{-1} s^{-1}]
ρ	salt density [kg m^{-3}].

Several types of direct-contact methods may be used to carry out these processes including spray columns, falling film columns, plate columns, and packed columns. Packed columns are especially effective if low pressure drop or low liquid holdup is important and high volumetric efficiency is needed. They are especially useful for corrosive gas or liquid service or for high-temperature applications in which plate column internals are not available. Thus, packed columns offer important advantages and are employed in a number of industrial applications, especially those involving high-temperature, high-pressure service.

An example of an irrigated packed bed is shown in Fig. 1. This direct contact heat exchanger (DCHX) uses molten salt to heat air for a solar thermal central receiver application. Salt is introduced at the top of the packed bed and distributed over the packing elements. It then flows over the packing surface in rivulets and contacts the upward-flowing air that has been introduced at the bottom of the column.

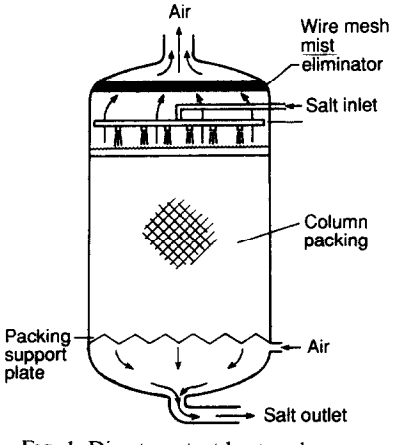

FIG. 1. Direct-contact heat exchanger.

A counterflow DCHX (the preferred method of operation) is perhaps somewhat more difficult to operate than some of the other columns because of flooding constraints. Flooding occurs when the counterflowing gas stream begins to carry liquid upward. Excessive pressure drop and loss of liquid develop, and heat and mass transfer rates decrease because liquid is poorly distributed. Thus, it is important to be able to predict not only pressure drop in the heat exchanger but also allowable operating conditions in which flooding will be avoided. These predictions are generally made on the basis of empirical correlations that usually have not been tested for a wide range of operating conditions or heat transfer fluids.

Similarly mass and especially heat transfer coefficients are predicted based on empirical correlations developed from data from a few simple gas/liquid systems. So, not only is it difficult to predict operating conditions with confidence for the DCHX, but it is also difficult to predict heat transfer rates with confidence. This situation has led to less use of the DCHX than is warranted given the advantages the technology offers.

The preceding list of energy-related applications of DCHX demonstrates the wide applications this technology offers in energy recovery, conversion, collection, and management. The technology could be used much more efficiently and widely if existing correlations for predicting heat transfer and pressure drop in a DCHX could be shown to work reliably for a wide range of operating conditions and heat transfer fluids.

The objective of the research described herein is to improve confidence in predictive methods for heat

transfer and pressure drop in a DCHX. To this end, we present experimental data on heat transfer and pressure drop in a DCHX operating with preheated atmospheric-pressure air as the coolant and molten nitrate salt as the heating medium. Tests were performed over a range of salt inlet temperatures to test the influence of fluid property variations and the influence of radiative heat transfer. Data for high operating temperatures and an unusual working fluid (molten salt) provide a more rigorous test of models than have previous experimental data. The full range of permissible air flow and salt flow rates were tested. These experimental data are compared with results from pressure drop and heat transfer models, and the validity of these models is thereby established.

2. PREVIOUS WORK

Most available studies on modeling irrigated packed-bed heat transfer rely on mass transfer correlations and the analogy between heat and mass transfer. None of the available models of direct-contact heat exchange include all aspects of the problem that are important in this study, namely, simultaneous liquid and gas flow (irrigated bed), low-pressure-drop commercial packings, high-temperature operation, and molten salt working fluids whose properties differ substantially from those of liquids typically used in irrigated packed-bed experiments. Standish and Drinkwater [1] presented data on heat transfer between hot gases and mercury or cerrobend in a packed bed. Fair [2] and Bravo and Fair [3] used the analogy between heat transfer and mass transfer to predict heat transfer rates in a packed bed given mass transfer coefficients. Balakrishnan and Pei [4, 5] developed a model of heat exchange between a gas and spherical particles in a packed bed. Dixon [6] modeled the thermal resistance of a packed bed with gas flow and used a simplified method to include radial terms. Mackey and Warner [7] used the analogy to predict heat transfer rates in a packed bed with downflowing liquid metals and upflowing gases.

Although the work done by Mackey and Warner is useful for liquid metal/gas systems, it is not sufficiently general to apply to other systems. For example, their direct mechanism, which was estimated from mass transfer data, is not applicable to molten salts because salt/vapor mass transfer coefficients have not been measured (because of their exceedingly low vapor pressure and because their vapors are unimportant to industry). Moreover, Mackey and Warner's equations for heat transfer do not allow us to determine when radiation is important or why the different packing materials contribute differently to the direct and indirect mechanisms.

Huang and Fair [8] measured heat transfer rates in a packed bed with a mineral spirits/air system and used the heat transfer/mass transfer analogy to predict the rates. They found that the analogy always underpredicted the experimentally determined rates; they attributed this to heat transfer by conduction in the packing (from wet to dry areas), which cannot be accounted for in mass transfer correlations.

In general, researchers measure the heat transfer rate as a function of the liquid and gas rates as well as the packing type. The resulting correlation is probably good for the system tested, but its application to other fluids is questionable. Table 1 presents a list of studies in which these types of correlations have been developed.

The problems associated with the extended use of correlations generated solely for a particular system can be demonstrated by the following comparison. Both Huang and Fair [8] and Pohlenz [9] gave correlations of experimental data relating the volumetric heat transfer coefficient, Ua, to gas rate and liquid rate, G and L, for air/oil systems with 1 in. ceramic Raschig rings (dimensions for Ua are lb h^{-1} $ft.^{-2}$ and for G and L, Btu h^{-1} $ft.^{-2}$):

$$\text{Huang and Fair: } Ua = 0.00026\, G^{1.69} L^{0.514}$$

$$\text{Pohlenz: } Ua = 0.083\, G^{0.94} L^{0.25}.$$

Even for these two very similar systems, we see large discrepancies in determining Ua, e.g. a factor of 4 or more. Possible explanations for the discrepancies include experimental error or a difference in liquid properties. Experimental errors in determining Ua for an irrigated packed column are discussed in ref. [10] and can be very large because of close approach temperatures at the top of the column. Liquid properties are not explicit in the above correlations, further demonstrating their limited usefulness for general prediction of heat transfer.

In an attempt to circumvent many of the limitations of the predictive methods previously discussed, an empirical model for heat transfer in an irrigated packed bed was presented in ref. [11]. Because the application of interest involved high temperatures, radiation heat transfer was included. Convection heat transfer was determined from a published correlation for mass transfer for the fraction of bed packing wetted by the liquid. Convection from the dry parts of the packing to the gas was also accounted for by incorporation of a fin-effect type of analysis and published correlations for heat transfer in packed beds with gas flow. A scaling analysis showed that for all conceivable applications of interest, radiation heat transfer can be neglected. One objective of the present work is to test the validity of this empirical model.

The pressure drop and flooding point in irrigated packed beds are estimated with empirical correlations. White [12] provides one of the earliest data sets, but he did not present a correlation of his data because he felt that much more data was needed. He measured pressure drop and determined flooding in a 150 mm column with Raschig rings and an air/water system. Sherwood *et al.* [13] developed a correlation based on the experimental data available at that time. They showed that the square of the superficial flooding

Table 1. Empirical correlations for irrigated packed bed heat transfer

Reference	System	Column diameter (cm)	Packing
Bennett [26]	air/oil	20.3	Raschig rings, 1.27 cm
Hujsak [27]	air/oil	20.3	Raschig rings, 1.27 cm
Pohlenz [9]	air/oil	20.3	Raschig rings, 2.54 cm
McAdams *et al.* [28]	air/water	10.2	Raschig rings, 2.54 cm
Yoshida and Tanaka [29]	air/water	25.4	Raschig rings, 2.54, 3.81 cm
Keey [30]	air/oil	10.2	Raschig rings, 1.97 cm
Nemunaitis and Eckert [31]	air/water	76.2	Pall rings, 5.08 cm

velocity correlated with the ratio of liquid and gas rates. A modified version of the Sherwood correlation provided by Leva [14] and others sees wide usage today. Sarchet [15] compared the two popular methods of determining the flooding point: visual and pressure-drop measurement. He reported that for small packing the two methods give comparable results, but for packing 2.45 cm and larger the visual flooding velocity may be 20% below the value determined by measuring the pressure drop.

Standish [16] modified the Sherwood correlation to include the effect of packing shape via the sphericity, which was defined as a packing shape parameter. Inclusion of this empirical shape factor improved the agreement between Standish's data and the Sherwood correlation for glass spheres and coke particles in an air/water system. They hypothesized that flooding is caused mainly by pressure gradients in the gas stream that would be influenced by the path the gas must follow through the bed.

Szekely and Mendrykowski [17] measured flooding criteria for mercury and nitrogen in a 2 in. column packed with glass beads, ceramic cylinders, and saddles. They found that the data fell about an order of magnitude low on the Leva correlation, but agreement with the original Sherwood correlation was quite good. The discrepancy was attributed to the high density and surface tension of the liquid. These results point out that the pressure-drop and flooding correlations are based on a relatively small set of gas/liquid systems, and extrapolation of the correlations to new systems can lead to large errors.

Buchanan [18]; Hutton *et al.* [19]; Bemer and Kalis [20]; and Stichlmair *et al.* [21] attacked the flooding problem from a different angle. They related the column pressure drop and flooding to the liquid holdup in the bed. In particular, Hutton *et al.* determined the flooding point as the point at which the gradient of liquid rate with holdup is zero. This approach met with partial success by satisfactorily predicting flooding for stacked rings but resulted in large errors for random rings. Buchanan, and Bemer and Kalis provide empirical equations that relate the column pressure drop to the holdup and a constant that is characteristic of the packing type and size. Bravo *et al.* [22] successfully used the Bemer and Kalis pressure-drop equation to calculate the pressure drop in eight sizes of structured packings from two manufacturers in an air/water system and for a variety of organic liquids in their vapors. Stichlmair *et al.* [21] developed a particle model which assumed that the characteristic dimension of the particles was increased because liquid adhered to the particle surface. The resulting expression for the pressure drop was written in terms of the single-particle friction factor, the bed porosity, and liquid holdup. The model showed good agreement with a wide variety of experimental data. Because the models of Bemer and Kalis, and Stichlmair *et al.* agree favorably with experimental data, we chose to compare both models with the experimental data obtained in this study.

3. DESCRIPTION OF THE EXPERIMENTAL APPARATUS

Tests described in this paper were carried out with the apparatus shown schematically in Fig. 2. Figure 3 depicts the details of the direct-contact heat exchange column. A mixture of sodium nitrate and potassium nitrate (in a 60/40 wt% ratio, respectively) was used during testing. The thermophysical properties for this salt mixture are given in Table 2. This salt is currently under consideration as a heat transfer fluid and storage medium for solar thermal central received systems that produce electrical power via the steam Rankine cycle. Initial tests were conducted with the eutectic mixture of lithium/sodium/potassium carbonate, which is a candidate storage medium for temperatures in the range 500–900°C. We found that using this salt resulted in exceptionally high column pressure drop from the salt foaming in the column. Presumably, the much higher viscosity of the salt, ~12 cp at 500°C, is responsible for the foaming. During flow visualization tests the nitrate salt, with a viscosity of 1.3 cp at 500°C, did not produce any noticeable foaming over the gas and liquid rates of interest.

An inventory of approximately 1700 kg of molten salt is kept in the storage tank. The salt is pumped out of the tank into the test loop by a cantilever centrifugal pump. Salt flow rate is controlled with a valve welded to the outlet port of the pump housing and actuated from just above the pump mounting flange.

A 1 in. Schedule 40 pipe carries the salt to the inlet of the heat exchanger. Immediately downstream of

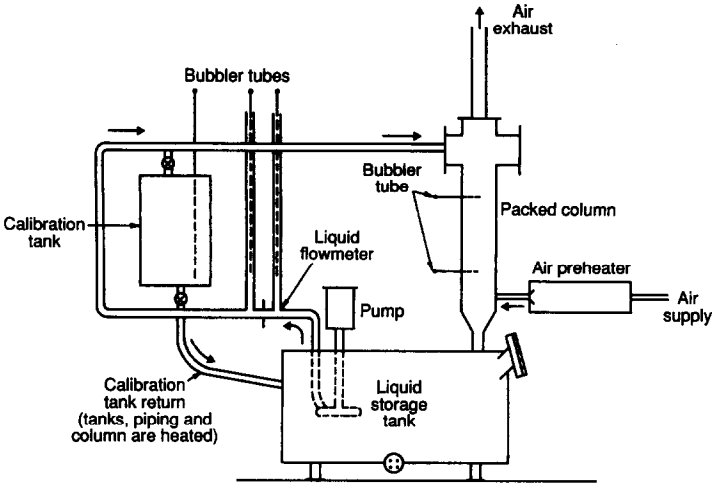

FIG. 2. Direct-contact heat exchange test loop.

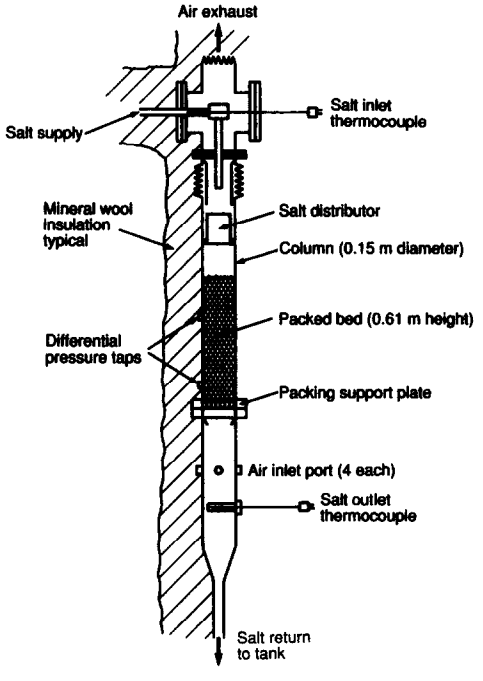

FIG. 3. Details of packed column used for direct-contact heat exchange experiments.

Table 2. Thermophysical properties of $KNO_3/NaNO_3$ equimolar mixture [32]. Data for the specific heat are for the eutectic, 54 mol% KNO_3 [33]

T (°C)	ρ (kg m^{-3})	$\mu \times 10^6$ (kg m^{-1} s^{-1})	k (W m^{-1} K^{-1})	C_s (J kg^{-1} K^{-1})
300	1899	3049	0.500	1711
350	1867	2350	0.510	1653
400	1836	1882	0.520	1593
450	1804	1555	0.530	1535
500	1772	1317	0.539	1476
550	1740	1138	0.549	1417

the pump, the salt flows through a calibrated orifice. Differential pressure across the orifice is sensed as the difference in height of salt in an open vertical pipe on either side of the orifice. A differential bubbler system is used to convert this difference in salt height to a voltage. Salt flow can be diverted into the calibration tank to allow calibration of the orifice flowmeter. As salt flows into this calibration tank, the increasing level in the tank is sensed by a bubbler. The rate of change in this bubbler output is compared with the output of the differential bubbler, which senses pressure difference across the orifice. Because the volume of the calibration tank is known as a function of height (by calibration with water), the rate of change of salt height in the calibration tank gives the volumetric flow rate directly.

For normal operation in which the salt is directed to the column, refer to Fig. 3. The salt enters the column top through a flange on the side of a large tee and then enters a small tee located inside the large tee. The smaller tee allows insertion of the calibrated chromel/alumel salt inlet thermocouple into the inlet stream and redirects the salt stream downward into the salt distributor. The salt distributor is an open-top can with three holes, each approximately 3 mm in diameter, in the bottom. Clearance between the vertical walls of the distributor and the inside diameter of the column is about 1 cm. We found that this distributor worked satisfactorily for flow rates between 60 and 180 cm^3 s^{-1}. Below 60 cm^3 s^{-1}, the salt issued irregularly from the three holes and tended to attach to the bottom of the distributor. Above 180 cm^3 s^{-1} the distributor tended to overflow. Within this flow range, three distinct streams issued cleanly from the distributor and spread uniformly over the top of the packed bed. These streams appeared to spread rapidly over the Pall rings within about 30 mm of the top of the bed.

Stainless steel Pall rings 15.9 mm in diameter and height were used in the column. A total height of

610 mm of randomly dumped rings was used, which produced a void fraction of 0.947 and a specific surface area of 341 $m^2\ m^{-3}$. A corrugated, perforated steel plate supported the rings at the lower column flange (Fig. 3). Two pressure taps located in the column wall were used with a differential bubbler system to measure column differential pressure during testing. The upper pressure tap was located about one column diameter below the top of the bed to ensure that the liquid and air flows were well distributed. The lower pressure tap was located about one column diameter above the bottom of the packed bed.

Preheated air was introduced into the bottom of the column about 300 mm below the packing support plate. An electric air preheater provided air temperatures up to about 380°C. Four symmetrically arranged inlet ports distributed the air at the base of the column to ensure uniform air flow. The air flow rate was measured with a calibrated ASME orifice flowmeter. The differential pressure was sensed with a Dwyer transducer. Air inlet temperature was measured with a chromel/alumel thermocouple inserted into the air inlet manifold.

Salt outlet temperature was measured with a calibrated chromel/alumel thermocouple inserted into a 25 mm (inside diameter) trough located below the air inlet ports. This trough was designed to ensure that the thermocouple that had just left the bottom of the packed bed would be bathed in salt.

All test loop piping was heated with tubular electrical heat trace, wrapped with stainless steel foil, and insulated with ceramic fiber insulation approximately 150 mm thick. The salt tank was heated with several flat-sheathed heaters attached to the tank bottom. The column was heated mainly with flat-sheathed heaters formed in a circular shape and attached to the column outside diameter with clamps.

All data, with the exception of the column differential pressure, were acquired with a Hewlett–Packard 3497 scanner controlled by a Hewlett–Packard Vectra microcomputer. Column differential pressure was read directly from a Merriam micromanometer.

4. TEST PROCEDURE

On the basis of a great deal of testing, we determined that the best comparison between the predictions of the heat transfer model and experimental data would be that of the heat transferred from the salt. In earlier attempts to measure the volumetric heat transfer coefficient, it was shown [10] that large uncertainties result, primarily because of the difficulty in measuring the air outlet temperature, which typically is very close to the salt inlet temperature. Measurement errors in the air stream are large because of radiation errors and because salt droplets are usually entrained in the air stream. Measuring the salt heat transfer is relatively simple, requiring only a measure of the salt flow rate and terminal salt temperatures. It is necessary, however, to account for salt heat transfer that occurs in regions of the column other than in the packed bed.

Included in these additional heat transfer paths are the heat lost from the salt to the column walls and the heat transferred to the air in the region below the packed bed. Because the air exiting the top of the packed bed is very nearly in thermal equilibrium with the salt entering from the salt distributor, we neglect salt-to-air heat transfer above the packed bed. Our experimental procedure allowed us to determine the loss from the salt to the column. The loss in the region below the packed bed was estimated and is included in our statement of experimental uncertainty. Data were reduced according to the following equation:

$$Q_{sm} = \dot{m}_s C_s (T_{si} - T_{so}) - Q_{loss}. \tag{1}$$

The term on the left-hand side of equation (1) is the heat transfer from the salt to the air, which occurs in the packed bed. The first term on the right-hand side is the salt heat loss determined from the measured salt flow rate and temperature drop. The second term on the right-hand side represents the two sources of heat loss from the salt stream just discussed and may be expressed as follows:

$$Q_{loss} = \dot{m}_s C_s (T_{si} - T_{so})|_{G=0} + Q_{outlet}. \tag{2}$$

Thus, the loss from the salt to the air in regions of the column other than the packed bed includes losses to the column wall, which is measured after every data point as described later, and heat loss below the packed bed, Q_{outlet}, which is estimated. It is the term on the left-hand side of equation (1) that we would like to deduce from the experimental data and compare with the heat transfer model.

The test loop was brought up to 400°C over approximately two days and left at that temperature for an additional day before testing again. During this period, a low flow of air was bled through the air preheater (which was turned on at a low power setting) and column to heat up the preheater and air piping. We then shut off the air flow and started the salt flow. After about 2 h, the salt and the column reached equilibrium as evidenced by the steadiness of the salt inlet and outlet temperatures. After this equilibrium was established, air flow was started again. Typically, a new equilibrium would be established within 10 min, again as evidenced by steady salt inlet and outlet temperatures. At this point, the data-acquisition system would be instructed to record 30 samples from each channel, to average each channel, and to calculate the standard deviation for each channel. Based on these average values, the gross heat loss from the salt could be calculated according to the first term on the right-hand side of equation (1).

After these data were recorded, the air flow was turned off. A new equilibrium would be reached within 3 min that corresponded to the heat loss from the salt through the column walls in the absence of air flow, e.g. the first term on the right-hand side of equation (2). The indicated column pressure differ-

ential under these conditions equals the bubbler offset signal because no air is flowing through the column to create a differential pressure. Again, 30 readings would be taken, and based on the average salt flow rate and salt inlet and outlet temperatures, the heat loss from the salt would be calculated and subtracted from the gross heat loss per equation (1). The column differential pressure recorded with air flow is reduced by the value recorded with no air flow to give the net column differential pressure. Standard deviation data were used to determine precision errors as described in the next section.

After establishing a higher air flow rate, the procedure would be repeated. The sequence of operating conditions usually included starting at low air flow and increasing the air flow in steps until the column differential pressure exceeded approximately 1000 Pa m^{-1} or until unsteady operation indicated the onset of flooding. Then, the air flow would be reduced in steps with the same salt flow. After this sequence was completed a new salt flow would be set and the procedure repeated. At each data point, operating conditions including air flow rate, salt flow rate, air inlet temperature, and salt inlet temperature were entered into the heat transfer and pressure-drop models. The predicted values of the salt heat transfer and column pressure drop were then determined for comparison with the data.

Initially, dry bed tests were conducted to determine the parameters required in the pressure-drop models of Bemer and Kalis [20] and Stichlmair *et al.* [21]. Dry pressure-drop data were taken over a gas flow range of 0.3–1.4 kg m^{-2} s^{-1} and a gas temperature range of 213–380°C. The fitting parameter ϕ in the model of Bemer and Kalis characterizing the packing type was found to be 0.83, which is in good agreement with the value of 0.80 given by Bemer and Kalis for Pall rings. The average dry-particle friction factor was also determined because single particle friction factor data for Pall rings were not available for the model of Stichlmair *et al.* The data and a least-squares curve fit procedure were used to evaluate the constants in a power law function relating the average dry-particle friction factor to the gas Reynolds number; the resulting expression is

$$f_0 = 6.508\, Re_g^{-0.241}.$$

The main test series involved simultaneous measurement of heat transfer and column differential pressure over a salt inlet temperature range of 334–520°C, salt flows ranging from 60 to 180 cm^3 s^{-1}, and air flows ranging from 280 to 1350 slpm. The minimum salt operating temperature was dictated by the tendency of the salt to freeze in the column during operation below 320°C. The maximum salt operating temperature was dictated by the desire to keep well below the salt decomposition temperature, 575°C, at which point it becomes excessively corrosive. Given the column inside diameter, the above flow rates correspond to liquid rates ranging from 6 to 18 kg m^{-2} s^{-1} and to air rates ranging from 0.3 to 1.4 kg m^{-2} s^{-1}. Resulting net salt heat transfer ranged from 480 to 4400 W. Resulting column differential pressure ranged from 160 to 1045 Pa m^{-1}. Generally, packed columns are operated above 400 Pa m^{-1} pressure drop, with 1200 Pa m^{-1} considered to be the point at which flooding commences. Thus, our range of operating conditions fully covered the operating map for a packed column. We did not explicitly measure the flooding point for this system. Based on the success of the pressure-drop correlations, we feel that existing flooding correlations are probably adequate.

5. UNCERTAINTY ANALYSIS

Referring to equation (1), the reported salt heat transfer rate was determined from the total heat transferred from the salt less column heat losses and the internal loss from the salt to the air below the packed bed. Because the column heat losses were determined after each data point, this bias error was measured and accounted for in the equation. The internal loss was estimated to be 3% of the gross salt heat transfer [23]. We include this loss as a negative bias error in determining the overall uncertainty in the heat transfer measurement.

Other uncertainties in equation (1) that must be considered include errors in the salt flow rate measurement, the specific heat of the salt, and the salt inlet-to-outlet temperature difference. By far, the largest contributor to the overall uncertainty is the problem in determining salt inlet-to-outlet temperature difference. The salt inlet and outlet temperatures were measured with chromel/alumel thermocouples which were manufactured from the same wire spool and were immersed in the salt in a similar manner. Thus, we expect any bias errors to be cancelled out when taking the difference between the salt inlet and outlet temperatures. A precision error in the temperature difference of 0.32°C was estimated based on temperature data recorded during an actual run.

Other errors in applying equation (1) include the salt flow rate measurement, $\pm 3.4\%$ bias error and 0.5% precision error, and the uncertainty in the salt specific heat, $\pm 3\%$ bias error. We determined that the total uncertainty in the measured salt heat transfer rate is $\pm 31\%$ at the high salt flow rates and $\pm 21\%$ at the low salt flow rates.

Input to the heat transfer model described in the next section is subject to uncertainties associated with the air flow rate, the salt and air inlet temperatures which are model inputs, and the air specific heat. By far, the largest error was the bias error introduced by radiation and convection effects on the air inlet thermocouple which caused the thermocouple temperature to deviate from the actual air inlet temperature.

The bias error in the air inlet temperature was estimated by devising a thermal resistance network characterizing the various heat transfer modes affecting

Table 3. Summary of uncertainties

Uncertainty source	Magnitude of uncertainty (%)
Measured salt heat transfer, low salt flow	21
Measured salt heat transfer, high salt flow	31
Calculated salt heat transfer	13
Measured column differential pressure	9

the air probe temperature. The thermal resistances included convection from the air to the probe, radiation from the probe to the pipe wall, convection from the air to the pipe wall, and conduction through the pipe insulation. Conduction in both the probe and pipe wall were found to be negligible. Analysis of the network showed that the probe temperature (measured temperature) always underpredicted the actual air temperature. The mean value of this bias error was 25°C. We used these results to eliminate the bias error in the air temperature from the data.

We also determined that the air flow rate measurement contributed a $\pm 1.1\%$ bias error and a 2.4% precision error. Air specific heat estimation contributed a $\pm 0.5\%$ bias error. We estimated that the salt inlet temperature measurement has a ± 3°C bias error and a 0.1°C precision error. After correcting the air inlet temperature as described above, we estimated a residual bias of ± 10°C and a precision error of 0.1°C. Based on these values, we estimate that the total uncertainty in the calculated salt heat transfer rate is $\pm 13\%$.

Column differential pressure was measured with a bubbler system as discussed earlier. This bubbler was calibrated against a micromanometer, which has a range of ± 5000 Pa and a resolution of 0.25 Pa. As described in Section 4 the column differential pressure was measured before the air flow was started to get the bubbler bias for zero air flow. This source of bias error was therefore eliminated. Based on the curve fit of the calibration data and the precision errors during an actual run, we estimate that the overall uncertainty in the column differential pressure measurement is $\pm 9\%$.

The uncertainties are summarized in Table 3.

6. RESULTS

6.1. *Pressure drop*

Pressure drop data were taken simultaneously with heat transfer data over a wide range of temperatures and flow parameters for comparison with packed-bed pressure-drop models of Bemer and Kalis [20] and Stichlmair *et al.* [21]. The comparisons were conducted to ensure that the column was operating properly (i.e. no channelling) and to determine how well each model agreed with the data. The results of this comparison are presented in Fig. 4. In total, 59 data points are included. The measured pressure drop is compared with the predicted pressure drop in the figure. The predicted pressure drop was determined from both the Bemer and Kalis model and the Stichlmair *et al.* model using the indicated liquid and gas flow rates and using properties of the two fluid streams determined at the average of their inlet and outlet temperatures. In the case of $L = 0$, air properties were determined at the air inlet temperature. Critical properties of the packing used during the tests, which are needed in one or both models, include the specific surface area and the void fraction and are given in Section 3.

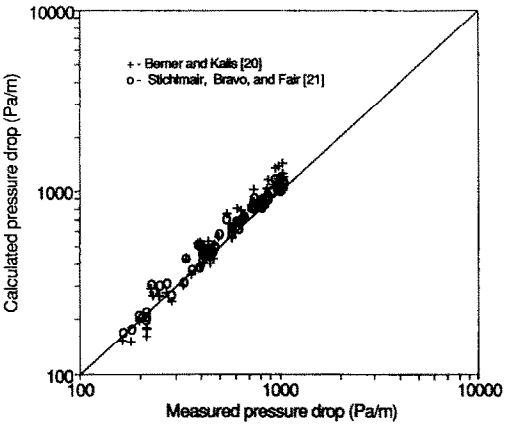

FIG. 4. Comparison of measured and predicted column pressure drop. Predictions are from the models of Bemer and Kalis [20] and Stichlmair *et al.* [21].

The parity plot in Fig. 4 shows that both models agree quite well with the experimental data. The standard deviation in the model of Stichlmair *et al.* was 9.4%; that for the model of Bemer and Kalis was 16.4%. It should be noted that the model of Bemer and Kalis was modified for a system with partially wetted packing. The fraction of wetted packing was evaluated using the model given by Onda *et al.* [24]. Bemer and Kalis found that data in the literature fell within $\pm 20\%$ of their model for metal Pall rings ranging in size from 15 to 50 mm. Stichlmair *et al.* also compared their model with data in the literature for 35 mm ceramic Pall rings. Even though their model appeared to agree very well with the data, no standard deviation was given in their paper. Note that the agreement of both models with the data given in this paper is good even for a pressure drop as high as 1045 Pa m^{-1}, which represents a point just prior to column flooding. We recommend using the model of Stichlmair *et al.* because (1) it is based on dry single-particle properties or in this case, average dry-bed properties which make the pressure drop easy to calculate and (2) it shows better agreement with our data.

6.2. *Heat transfer*

The heat transfer model with which we compared our experimental data is a modification of the model

given in ref. [11]. In its original form, this model used the mass transfer correlation of Onda *et al.* [24] and the mass transfer/heat transfer analogy to determine the convective heat transfer coefficient at the liquid/gas interface. At the gas/dry packing interface the packed-bed correlation of Whitaker [25] was used. However, in comparing the film coefficients predicted by these two correlations, we found that the Whitaker values were about three times larger than those predicted by the Onda *et al.* correlation. The reason for the large discrepancy was not determined. Because the unwetted area fraction is fairly small, the overall heat transfer is affected by only 1–2%. However, it does tend to produce a dependence on wetted fraction which is counterintuitive: it gives increasing heat transfer with decreasing wetted fraction. For this reason, we chose to use the Onda correlation to give convective heat transfer film coefficients both at the liquid/gas interface and at the gas/dry packing interface. Physically, this seems reasonable because the primary resistance at the liquid/gas interface is in the gas film, and the hydrodynamic conditions in the gas film at the liquid/gas interface and the gas/dry packing interface should be similar.

As described previously, we have found that direct contact heat exchangers typically operate with very close approach temperatures, e.g. $T_{ao} \approx T_{si}$. This implies that the effectiveness of the heat exchanger is near unity. In order to test this idea, the heat transfer model described previously was used to compare detailed heat exchanger analyses with a simplified analysis in which the heat exchanger was assumed to operate as a counterflow heat exchanger with effectiveness of unity. In this case the heat transferred from the salt can be calculated from

$$Q_s = GA_cC_{pa}(T_{si} - T_{ai}). \quad (3)$$

For operating conditions corresponding to all of the heat transfer tests, we found that the above equation deviated with results obtained from the detailed analysis by less than 0.5%. This means that the performance of the direct-contact heat exchanger can be calculated very simply with equation (3), and this method will be used to present heat transfer data in this section. If the heat transfer data agree with the model, the very high effectiveness of a direct-contact heat exchanger will have been demonstrated.

Figure 5 presents a comparison of the measured salt heat transfer with the calculated salt heat transfer in the form of a parity plot. As discussed previously, the operating conditions for each experimental point were entered into equation (3) to predict the expected salt heat transfer for those operating conditions. The results in Fig. 5 demonstrate that the comparison is quite good. Overall, for the 59 data points plotted, the standard deviation between the predicted and measured values is 25%. A total of 61 runs were made; two were discarded. As in previous studies (e.g. ref. [23]) we found that the liquid flow rate had little influence on the heat transfer.

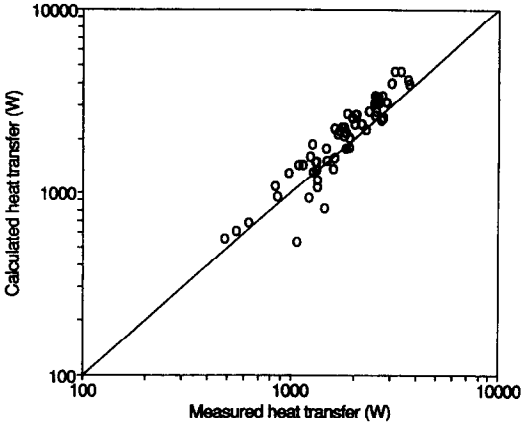

FIG. 5. Comparison of measured and predicted heat transfer.

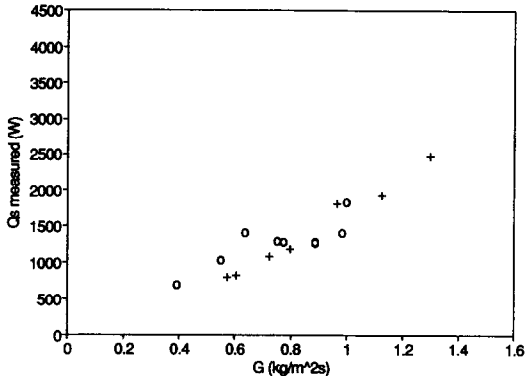

FIG. 6. Effect of operating temperature on heat transfer. $L = 12$ kg m^{-2} s^{-1}: +, $T_{si} = 340$°C, $T_{ai} = 216$°C; ○, $T_{si} = 506$°C, $T_{ai} = 378$°C.

Figure 6 shows the relative importance of radiation heat transfer in the direct-contact heat exchanger. In this figure, the measured salt heat transfer for a fixed salt flow rate is plotted against air rate for two sets of air and salt temperatures. For both data sets the inlet temperature difference $(T_{si} - T_{ai})$ was 120°C. However, the air and salt temperatures were increased by 160°C between these data sets. On the basis of the scaling analysis of ref. [23], one would expect an increase of 120% in the radiative heat transfer component relative to the convective heat transfer for this increase in air and salt inlet temperatures at a fixed temperature difference. Within experimental uncertainties, Fig. 6 shows that there is essentially no effect of this change in temperature on the measured salt heat transfer. Therefore, the data indicate that radiation heat transfer is negligible in the direct-contact heat exchanger. This is also consistent with the findings of Mackey and Warner [7].

7. CONCLUSIONS

Pressure drop and direct-contact heat transfer between a preheated stream of air and a stream of molten nitrate salt in a packed bed were measured

and compared with empirical models. The range of gas rates and resulting pressure drop fully covered the operating range for irrigated packed beds. The heat transfer model and experimental data agree to within the uncertainty in the empirical correlations used to produce the model and the experimental uncertainties. Agreement between a model for the pressure drop in the packed bed and the experimental data was also good. The contribution of radiation heat transfer was found to be negligible. The heat exchanger effectiveness was essentially unity, e.g. the heat exchanger was found to operate as a simple counterflow exchanger of infinite number of transfer units.

Because a commercial heat exchanger would most likely operate with significantly lower liquid rates than those presented in this work, a range of liquid rates needs to be tested to fully validate the model. Reduced liquid rates will result in less wetted surface area thereby enhancing the importance of conduction in the packing. Different packings should also be tested to make sure that the treatment of conduction heat transfer in the packing is valid. Finally, testing at a larger scale is required before the model can be fully validated and before acceptance of the concept can be expected by practising engineers.

Acknowledgment—The work described in this paper was supported by the Oak Ridge National Laboratory under Subcontract 10X-SD344V. Support for L. W. Swanson was provided by the Associated Western Universities.

REFERENCES

1. N. Standish and J. Drinkwater, The effect of particle shape on flooding rates in packed columns, *Chem. Engng Sci.* **25,** 1619–1621 (1970).
2. J. R. Fair, Designing direct contact coolers/condensers, *Chem. Engng* 91–100 (June 1972).
3. J. L. Bravo and J. R. Fair, Generalized correlations for mass transfer in packed distillation columns, *Ind. Engng Chem. Process Des. Dev.* **21,** 162–170 (1982).
4. A. R. Balakrishnan and D. C. T. Pei, Heat transfer in gas–solid packed bed systems. 2. The conduction mode, *Ind. Engng Chem. Process Des. Dev.* **18**(1), 40–46 (1979).
5. A. R. Balakrishnan and D. C. T. Pei, Heat transfer in gas–solid packed bed systems. 3. Overall heat transfer rates in adiabatic beds, *Ind. Engng Chem. Process Des. Dev.* **18**(1), 47–50 (1979).
6. A. G. Dixon, Thermal resistance models of packed-bed effective heat transfer parameters, *A.I.Ch.E. Jl* **31**(5), 826–834 (1985).
7. P. J. Mackey and N. A. Warner, Heat transfer between dispersed liquid metals and gases in packed beds, *Metall. Trans.* **3,** 1807–1816 (1972).
8. C. C. Huang and J. R. Fair, Direct-contact gas liquid heat transfer in a packed bed, *Heat Transfer Engng* **10**(2), 19–28 (1989).
9. J. B. Pohlenz, Heat and mass transfer in packed towers, Ph.D. Thesis, Massachusetts Institute of Technology, Cambridge, Massachusetts (1947).
10. M. S. Bohn, Air/molten salt direct-contact heat-transfer, *J. Solar Energy Engng* **197,** 208–214 (1985).
11. M. S. Bohn, Analytical model of an irrigated packed-bed direct contact heat exchanger at high temperature, *Proc. 2nd ASME–JSME Thermal Engng Conf.*, Honolulu, Hawaii (1987).
12. A. White, Pressure drop and loading velocities in packed towers, *Trans. Am. Inst. Chem. Engrs* **31,** 390–408 (1935).
13. T. K. Sherwood, G. H. Shipley and F. A. Holloway, Flooding velocities in packed columns, *Ind. Engng Chem.* **30,** 765–769 (1938).
14. M. Leva, Flow through irrigated dumped packings, *Chem. Engng Prog. Symp. Ser.* **50,** 51–59 (1954).
15. B. R. Sarchet, Flooding velocities in packed towers, *Trans. Am. Inst. Chem. Engrs* **38,** 283–304 (1942).
16. N. Standish, Heat transfer in liquid metal irrigated packed beds countercurrent to gases, *Trans. Metall. Soc. AIME* **242,** 1733–1740 (1968).
17. J. Szekely and J. Mendrykowski, On the flooding criteria for liquids with high density and high interfacial tension, *Chem. Engng Sci.* **27,** 959–963 (1972).
18. J. E. Buchanan, Pressure gradient and liquid holdup in irrigated packed towers, *I&EC Fundam.* **8,** 502–511 (1969).
19. B. E. T. Hutton, L. S. Leung and P. C. Brooks, On flooding in packed columns, *Chem. Engng Sci.* **29,** 493–500 (1974).
20. G. G. Bemer and G. A. J. Kalis, A new method to predict hold-up and pressure drop in packed columns, *Trans. Instn Chem. Engrs* **56,** 200–204 (1978).
21. J. Stichlmair, J. L. Bravo and J. R. Fair, General model for prediction of pressure drop and capacity of countercurrent gas/liquid packed columns, *Gas Separation Purification* **3,** 19–28 (1989).
22. J. L. Bravo, J. A. Rocha and J. R. Fair, Pressure drop in structured packings, *Hydrocarbon Processing* 45–49 (March 1986).
23. M. S. Bohn, Heat transfer and pressure drop measurements in an air/molten salt direct-contact heat exchanger, SERI/TP-253-3426, Solar Energy Research Institute, Golden, Colorado (1988).
24. K. Onda, H. Takeuchi and Y. Koyama, Effect of packing materials on the wetted surface area, *Kagaku Kogaku* **31,** 126–134 (1967).
25. S. Whitaker, Forced convection heat transfer correlations for flow in pipes, past flat plates, single cylinders, single spheres, and for flow in packed beds and tube bundles, *A.I.Ch.E. Jl* **18**(2), 361–371 (1972).
26. G. A. Bennett, M.S. Thesis, Case Institute (1941).
27. K. L. Hujsak, The transfer of heat between air and a nonvolatile oil in a packed tower, M.S. Thesis, Massachusetts Institute of Technology, Cambridge, Massachusetts (1947).
28. W. H. McAdams, J. B. Polhenz and R. C. St John, Transfer of heat and mass between air and water in a packed tower, *Chem. Engng Prog.* **45,** 241–252 (1949).
29. F. Yoshida and F. Tanaka, Air–water contact operations in a packed column, *Ind. Engng Chem.* **43,** 1467–1473 (1951).
30. R. B. Keey, Fluid–fluid heat transfer in a packed column, *Proc. Third Int. Heat Transfer Conf.*, Vol. 4, pp. 322–328 (1966).
31. R. R. Nemunaitis and J. S. Eckert, Heat transfer in packed towers, *Chem. Engng Prog.* **71,** 60–67 (1975).
32. R. W. Bradshaw and R. W. Carling, A review of the chemical and physical properties of molten alkali nitrate salts and their effects on materials used for solar central receivers, SAND87-8005, Sandia National Laboratory (1987).
33. Anon., Physical property data compilation relevant to energy storage, NSRDS-NBS 61, Part II, National Bureau of Standards (1979).

COMPARAISON DE MODELES ET DE DONNEES EXPERIMENTALES POUR LA PERTE DE PRESSION ET LE TRANSFERT THERMIQUE DANS LES LITS FIXES IRRIGUES

Résumé—On présente une comparaison de données expérimentales avec des modèles d'échange de chaleur et de perte de pressin dans des lits fixes irrigués en s'intéressant à la validité des modèles, à l'importance du transfert radiatif et à l'efficacité. Le transfert thermique et la perte de pression sont mesurés dans une colonne de 150 mm de diamètre avec un lit d'anneaux métalliques Pall haut de 610 mm. Les fluides de travail sont le sel de nitrate fondu et l'air préchauffé. Les températures d'entrée du sel varient de 335 à 520°C et celles de l'air de 215 à 380°C. On fait la comparaison avec une version modifiée du modèle de Bohn (*Proc. 2nd ASME–JSME Thermal Engng Conf.*, Honolulu, Hawaii (1987)). Pour les débits testés d'air 0,3–1,4 kg m^{-2} s^{-1} et de sel 6–18 kg m^{-2} s^{-1}, les données s'accordent au modèle avec 25% de déviation standard. Le rôle du transfert radiatif est relativement minime et le transfert est celui d'un échangeur à contre-courant avec une efficacité unité. La perte de pression s'étendant entre 160 et 1045 Pa m^{-1}, la déviation standard est de 9,4% pour le modèle de Stichlmair *et al.* (*Gas Separation Purification* **3**, 19–28 (1989)) et de 16,4% pour celui de Bemer et Kalis (*Trans. Instn Chem. Engrs* **56**, 200–204 (1978)).

EIN VERGLEICH BERECHNETER UND GEMESSENER ERGEBNISSE FÜR DRUCKABFALL UND WÄRMEÜBERGANG IN BERIESELTEN SCHÜTTUNGEN

Zusammenfassung—In dieser Arbeit wird über einen Vergleich zwischen berechneten und gemessenen Ergebnissen für den Wärmeaustausch und den Druckabfall in berieselten Schüttungen berichtet, wobei besonderer Wert auf die Validierung des Modells, die Bedeutung des Strahlungswärmeaustausches und die Wirksamkeit eines solchen Wärmeaustauschers gelegt wird. Die Messungen werden in einer Säule mit 150 mm Innendurchmesser und einer 610 mm hohen Schüttung aus Metallringen ausgeführt. Als Arbeitsfluide dienen geschmolzenes Nitratsalz und vorgewärmte Luft. Die Eintrittstemperaturen liegen zwischen 335 und 520°C bzw. 215 und 380°C. Die Versuchsergebnisse für den Wärmeübergang mit Salz werden mit Rechenergebnissen aufgrund einer modifizierten Version des Wärmeübertragungsmodells von Bohn verglichen (*Proc. 2nd ASME–JSME Thermal Engng Conf.*, Honolulu, Hawaii (1987)). Im Bereich der untersuchten Massenstromdichten für Luft und Salz (0,3–1,4 kg m^{-2} s^{-1} bzw. 6–18 kg m^{-2} s^{-1}) stimmen die Meßwerte innerhalb 25% Standardabweichung mit dem Modell überein. Es zeigt sich, daß die Wärmeübertragung durch Strahlung eine verhältnismäßig geringe Rolle spielt, und daß sich der Wärmeübertrager im wesentlichen wie ein einfacher Gegenstromwärmeübertrager mit dem Wirkungsgrad 1 verhält. Die Meßwerte für den Druckabfall liegen im Bereich zwischen 160 und 1045 Pa m^{-1}, sie werden mit zwei Modellrechungen verglichen. Die Standardabweichung bei Verwendung des Modells von Stichlmair *et al.* (*Gas Separation Purification* **3**, 19–28 (1989)) beträgt 9,4%, bei Verwendung des Modells von Bemer und Kalis (*Trans. Instn Chem. Engrs* **56**, 200–204 (1978)) beträgt sie 16,4%.

СРАВНЕНИЕ МОДЕЛЕЙ И ЭКСПЕРИМЕНТАЛЬНЫХ ДАННЫХ ПО ПЕРЕПАДУ ДАВЛЕНИЯ И ТЕПЛОПЕРЕНОСУ В ФИЛЬТРУЕМЫХ УПАКОВАННЫХ СЛОЯХ

Аннотация—Проводится сравнение экспериментальных данных и моделей теплопереноса и перепада давления в фильтруемых упакованных слоях. Особое внимание уделяется определению адекватности моделей, роли радиационного теплопереноса и эффективности теплообменников. Теплоперенос и перепад давления определялись в столбе с внутренним диаметром 150 мм, заполненном слоем металлических колец Пэлла высотой 610 мм. Рабочими жидкостями являлись расплавленная азотнокислая соль и нагретый воздух. В экспериментах использовались температуры соли на входе, изменяющиеся в диапазоне 335–520°C, и температуры воздуха на входе в интервале 215–380°C. В случае соли проводится сравнение экспериментальных данных и модифицированного варианта модели теплопереноса, разработанной Боном (*Proc. 2nd ASME–JSME Thermal Engng Conf.*, Honolulu, Hawaii (1987)). Данные, полученные в исследуемых диапазонах расходов воздуха и соли (0,3–1,4 кг $м^{-2}$ $с^{-1}$ для потока воздуха и 6–18 кг $м^{-2}$ $с^{-1}$ для потока соли), согласуются с моделью с точностью до 25%. Найдено, что родь радиационного теплопереноса является сравнительно несущественной и данный теплообменник аналогичен простому противоточному теплообменнику с эффективностью теплообмена порядка единицы. Результаты обеих моделей для перепада давления в столбе сравниваются с экспериментальными данными, полученными в диапазоне от 160 до 1045 Па $м^{-1}$. Стандартное отклонение для модели Стильмейра (*Gas Separation Purification* **3**, 19–28 (1989)) составляет 9,4%, для модели Бемера и Калиса (*Trans. Instn Chem. Engrs* **56**, 200–204 (1978))—16,4%.